J Mater Sci (2007) 42:8320–8325
DOI 10.1007/s10853-006-0021-z

# Preparation and characterization of $Cu/SiO_2$ catalyst by co-gelation process

**Mingfang Zheng · Tianbo Zhao · Wenguo Xu · Fengyan Li · Yue Wang**

Received: 21 November 2005 / Accepted: 20 March 2006 / Published online: 28 June 2007


**Abstract** $Cu/SiO_2$ catalyst with bimodal pore structure was prepared by co-gelation reactions of tetramethoxysilane (TMOS) and copper nitrate in the presence of poly (ethylene oxide) (PEO) with an average molecular weight of 10,000 and the catalyst of acetic acid. In this process, the interconnected macroporous morphology was formed when transitional structures of spinodal decomposition were frozen by the sol–gel transition of silica. The addition of copper into the silica–PEO system had a negligible effect on the morphology formation. In gel formation, it was found that the crystallite sizes of the CuO estimated from the peak width in the $Cu/SiO_2$ with the presence of PEO were not small as expected. It was considered that there was no obvious interaction between the Cu cation and PEO, most of the copper ions in wet silica gel were present in the outer solution. They easily aggregated as copper salts in the drying process of wet gel and decomposed into CuO particles in heating. While in the $Cu/SiO_2$ with the absence of PEO, the Cu was selectively entrapped as small particles in the gel skeleton due to the interaction between Cu aqua complex and silica gel network.

M. Zheng · T. Zhao (✉) · W. Xu
Department of Chemistry, School of Science,
Beijing Institute of Technology, Beijing 100081, P.R. China
e-mail: zhaotb@bit.edu.cn

F. Li · Y. Wang
Department of Applied Chemistry,
Beijing Institute of Petrochemical Technology, Beijing 102617,
P.R. China

## Introduction

Supported copper catalysts are frequently employed in a variety of reactions such as methanol steam reforming [1], dehydrogenation [2], and ester hydrogenolysis [3]. To achieve high catalytic activity, it is necessary to disperse fine metal particles in well-defined pores in support. By conventional method for catalyst preparation such as impregnation, however, inhomogeneous aggregation of metal species at grain boundary of support occurs especially at higher metal content, and large size of metal particle results. Although heterogeneity of this type is easily suppressed by adopting sol–gel method, there is few research on preparation of Cu-containing catalyst by sol–gel method [4, 5]. On the other hand, Nakanishi et al. has developed a sol–gel process including phase separation to prepare continuous porous silica having double pore structures with micrometer-size macropores and nanometer-sized mesopores [6, 7]. As a first application of the material, they prepared a column for HPLC from a rod-type silica monolith with bimodal pore structure [8], and the column shows superior separation properties in HPLC analysis compared with conventional packed columns. In the bimodal porous silica, mesopores act as functional surfaces after surface modification, and macropores serve high-speed pathway to gas- and liquid-phases molecules to reach the surfaces in mesopores. Because of this advantage in the bimodal porous silica gel, it would have high potential in many applications other than HPLC, such as catalysis, adsorption, and separation and so on, where both molecular transportation and surface interaction concur.

Recently, macropore-tailoring by phase separation has been applied to mixed metal oxides, such as silica–titania, silica–zirconia, silica–alumina systems [9–11]. Silica–titania and silica–zirconia have shown improved character-

istics, such as zero thermal expansion, high alkali resistance and high mechanical strength. Silica–alumina has shown excellent catalytic activity in the cracking of cumene. Silica-supported nickel and palladium catalysts with both macropores and mesopores were also prepared [12, 13]. Pd–silica catalyst with mesopores of 12 nm and macropores of 2 μm has shown much higher activity than has a commercial palladium carbon catalyst without macropores.

In the present work, we apply the phase separation process to prepare $Cu/SiO_2$ catalyst by co-gelation reactions of tetramethoxysilane (TMOS) and copper nitrate in the presence of poly (ethylene oxide) (PEO) and the catalyst of acetic acid. Both the effect of Cu addition on the formation of the macroporous morphology and the effect of the procedure of Cu loading on the dispersion of Cu in the macroporous gel are investigated in detail.

## Experimental

### Sample preparation

TMOS (Wuhan University Silicone New Material Co.) and copper (II) nitrate trihydrate were used as silica and copper sources, respectively. PEO, with an average molecular weight of 10,000 (Beijing Chemical Reagent Co.) was used as the polymer component. Acetic acid was used as a catalyst for hydrolysis and polycondensation.

Sample gels were prepared by adding 28.4 mL of TMOS (98 mass%, 1.032 g/mL) to a solution containing PEO, copper nitrate and 52 mL of 0.01 mol/L acetic acid, and the mixture was then stirred for 30 min in air. The amounts of PEO and copper (II) nitrate trihydrate are summarized in Table 1. The resultant homogeneous solution was sealed in a plastic container, and kept at 50 °C for 24 h for gelation. The resultant wet gel was dried at 50 °C for 1 week and then heated at 500 °C for 2 h. The $CuO/SiO_2$ samples were reduced for 16 h in a flowing mixture of 25% $H_2/N_2$ (40 mL/min) at 220 °C to provide $Cu/SiO_2$.

A reference monolithic silica gel was prepared using a procedure described by Ishizuka et al. (denoted as Silica) [14]. The composition of the reaction mixture except for copper nitrate was same with silica gels prepared above in this work.

### Characterization of samples

A scanning electron microscope (SEM: JSM-35C, Japan) was employed to examine the morphology of samples on a micrometer scale. Macropore size was obtained by averaging more than five directly measured values on the SEM photographs. Nitrogen adsorption–desorption isotherms for $CuO/SiO_2$ samples were measured at –196 °C on an automatic adsorption-measurement system (AUTOSORB-1, USA). The specific surface area was calculated from the adsorption branch according to the Brenauer-Emmett-Teller (BET) method. The pore size distribution was calculated by the BJH method, and the adsorption branch was used to estimate the median pore size. The total pore volume was calculated from the amount of $N_2$ adsorbed at $P/P_0 > 0.95$. X-ray diffraction (XRD) patterns were recorded on a XRD-7000 (Shimadzu, Japan) using Cu-$K_\alpha$ radiation ($\lambda = 0.154$ nm) to detect the crystal structure of the samples. The particle size of metal oxide was estimated from full width at half maximum (FWHM) of diffraction peaks.

## Results

Table 1 summarizes some physical properties of $CuO/SiO_2$ samples prepared in the work. Figure 1 shows nitrogen adsorption–desorption isotherms and corresponding pore

**Table 1** Quantities of some reagents used in preparing silica-supported copper catalysts and some physical properties of catalysts

| Sample[a] | $Cu(NO_3)_2 \cdot 3H_2O$ (g) | PEO (g) | MS[b] (μm) | PV[c] ($cm^3/g$) | SA[d] ($m^2/g$) | PS[e] (nm) | CuO CS[f] (nm) |
|---|---|---|---|---|---|---|---|
| Silica | 0.0 | 5.0 | 6.1 | 0.83 | 455.5 | 7.3 | – |
| Cu-11 | 4.6 | 5.0 | 2.4 | 0.24 | 381.9 | 2.5 | 21 |
| Cu-14 | 5.8 | 5.0 | 2.2 | 0.19 | 321.0 | 2.4 | 26 |
| Cu-17 | 7.7 | 5.0 | 6.5 | 0.22 | 375.4 | 2.4 | 27 |
| Cu-20 | 9.2 | 5.0 | 9.3 | 0.19 | 330.9 | 2.3 | 24 |
| Cu-14R | 4.4 | 0.0 | 0.0 | 0.25 | 286.1 | 3.5 | 7 |

[a] Number represents the amount of metal oxide in the catalyst in wt.%

[b] MS, Macropore size for the calcined sample

[c] PV, The total pore volume for the calcined sample

[d] SA, Specific surface area for the calcined sample

[e] PS, Median pore size for the calcined sample

[f] CS, crystallite size. Estimated from XRD peak width at 35.1° according to Scherrer's equation

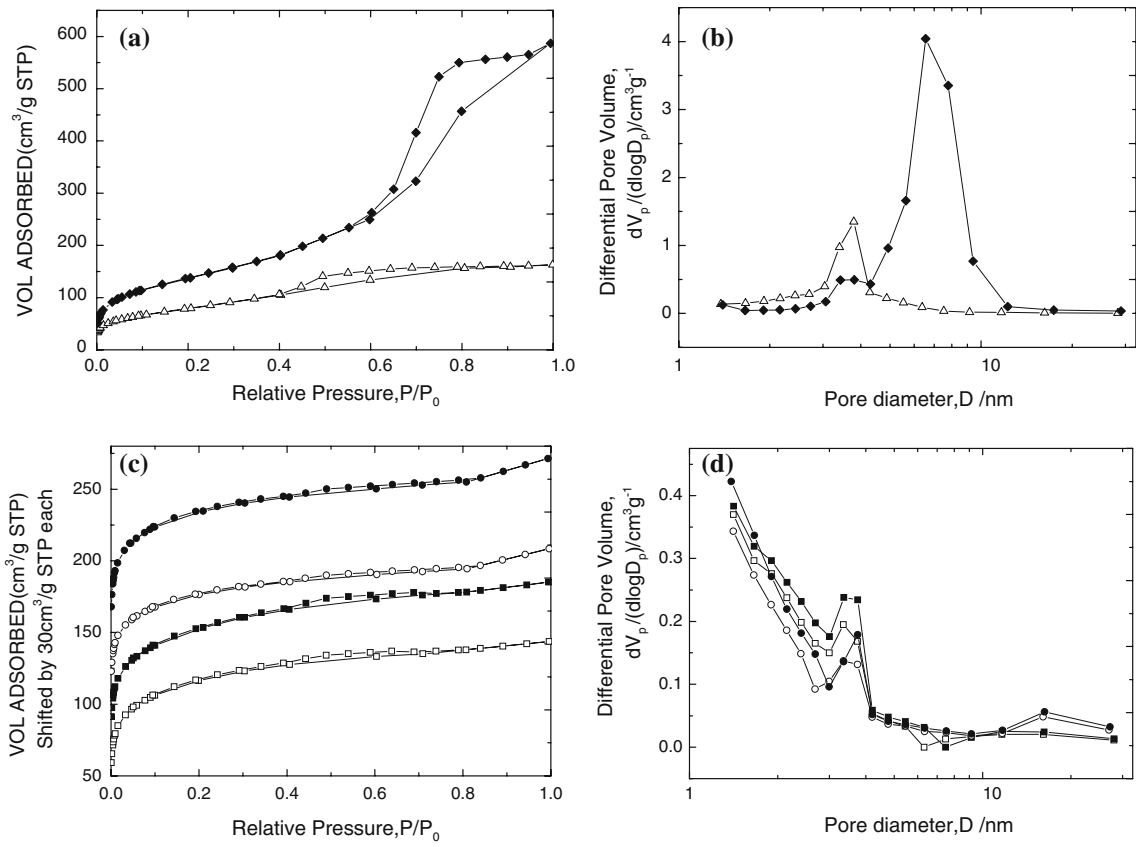


**Fig. 1** Nitrogen adsorption–desorption isotherms and corresponding pore size distribution of the gel samples. *Closed diamond*: Silica; *Open triangle*: Cu-14R; *Closed circle*: Cu-11; *Open circle*: Cu-14; *Closed square*: Cu-17; and *Open square*: Cu-20

size distribution of the samples. It can be found that the Silica exhibits type IV adsorption characteristic with H2 hysteresis loop. A well-defined step occurs at $P/P_0 = 0.6$–0.9, indicating the existence of mesopores; a little increases in adsorption until $P_0$, suggesting macropores are also present, while the Cu-14R with the absence of PEO has mesopores but no macropores (Fig. 1a). For the $CuO/SiO_2$ samples with the presence of PEO, capillary condensation at medium $P/P_0$ demonstrates the existence of mesopores. Limited but distinct adsorption at high relative pressures indicates the presence of macropores (Fig. 1c). The pore size distributions of the Silica and the Cu-14R are narrow, with main pores centering at ca. 7.3 nm and 3.5 nm (Fig. 1b), while relatively broad pore size distributions are observed for the $CuO/SiO_2$ samples in the presence of PEO (Fig. 1d). As shown in Table 1, BET surface area, the total pore volume and median pore size of the $CuO/SiO_2$ samples are smaller than those of the Silica.

Figure 2 shows the SEM micrographs for the calcined samples. All samples except for the Cu-14R have interconnected macropores, and macropore size varies with CuO content.

Figure 3 shows XRD profiles of the Cu-20 dried at 50 °C and calcined at 500 °C. The pattern for the Cu-20 dried at 50 °C is amorphous (Fig. 3a). After calcination, a diffraction pattern ascribed to CuO is observed for the Cu-20 sample (Fig. 3b). The patterns for other $CuO/SiO_2$ samples dried at 50 °C and calcined at 500 °C are similar to the Cu-20 (profiles not shown).

Figure 4 shows XRD profiles of the $CuO/SiO_2$ samples calcined at 500 °C. The peaks of CuO are observed for all the samples, and the FWHM of diffraction peaks slightly increases with increasing CuO content. A crystallite size estimated from the FWHM according to Scherrer's equation is summarized in Table 1. The crystallite size except for the Cu-20 slightly increases with increasing CuO content.

Figure 5 shows XRD profiles of reduced bodies of the samples shown in Fig. 4. Compared with the patterns in Fig. 4, the decrease in the intensity of CuO diffraction peaks is noticed from Cu-11 to Cu-20, but no new diffraction peaks are observed. This may be due to incomplete reduction of the bulk CuO or due to reoxidation of the $Cu^0$ species to $Cu^{2+}$.

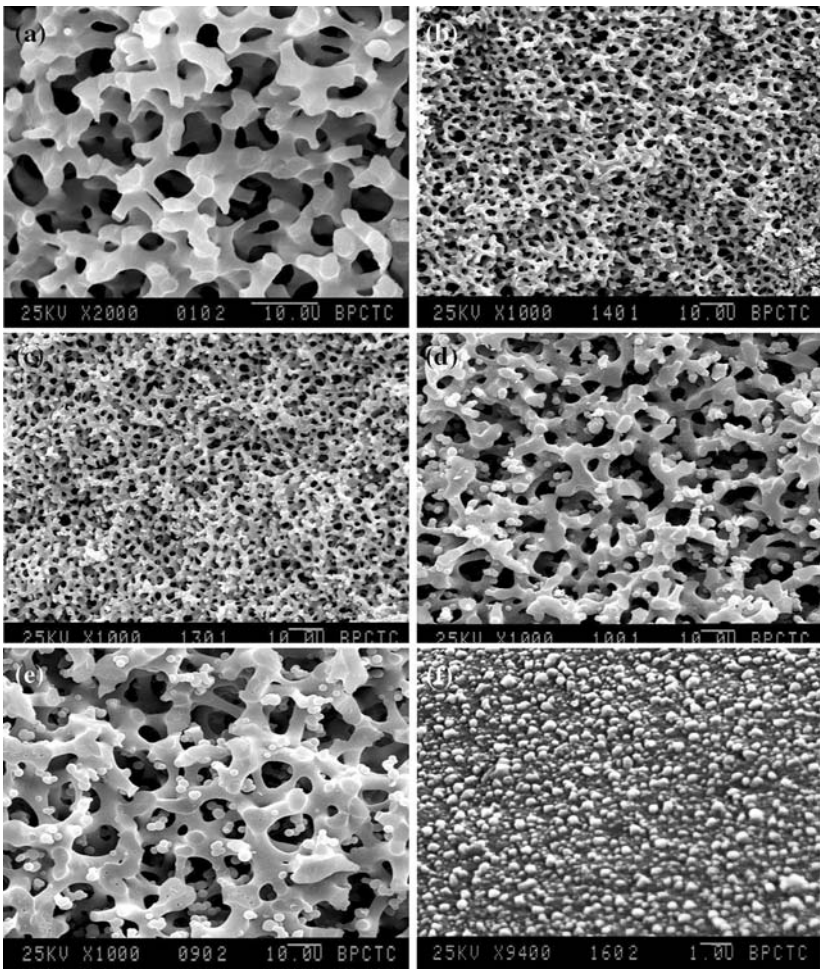


**Fig. 2** SEM micrographs of the calcined samples. (**a**) Silica, (**b**) Cu-11, (**c**) Cu-14, (**d**) Cu-17, (**e**) Cu-20, and (**f**) Cu-14R

## Discussion

### Structure formation of silica–copper in co-gelation process

For the pure silica system, the formation of a gel with an interconnected morphology in the micrometer range has been explained by the concurrence of phase separation and the sol–gel transition induced by the polymerization of an alkoxide-based silica [15, 16]. For the silica–metal system, the addition of metal to the silica system has different effect on the morphology formation. In a silica–zirconia system, the addition of zirconia to the silica system affects the electrostatic nature as well as the structure of the gel network developed in the sol–gel reaction. These changes largely affect the phase separation tendency of the system with poly (acrylic acid) (HPAA) in which the inorganic gel becomes the major component in a conjugate phase. However, the system with PEO is relatively insensitive to the change in the property of the inorganic phase. The domain size obtained changes markedly with only small changes in zirconia content [10]. In the silica–alumina and silica–nickel systems, the addition of alumina and nickel to the silica–PEO system has a negligible effect on the morphology formation [11, 12]. For the silica–titanium system, although the atomic absorption analysis of the finally heat-treated samples revealed that about half of the titanium has been lost during the treatments of solvent exchange, drying and heat treatment, the macroporous structure could be reproduced with both of HPAA and PEO without spoiling sharp distributions as in pure silica systems [9].

In the present silica–copper system, PEO is also preferable for control of the morphology. The morphology control in the silica–copper system is much like that in the silica–alumina systems. The sample Cu-14R has no interconnected macropores in the absence of PEO. At the compositional region, the macroporous morphology results are almost the same for both the $CuO/SiO_2$ samples and Silica in the presence of PEO (Fig. 2). Thus, it can be concluded that the addition of copper to the silica–PEO system also has a negligible effect on the morphology formation. On the other hand, the significant difference in the effect of the addition of metal oxides between alumina and copper oxide on the domain formation suggests the formation of gel

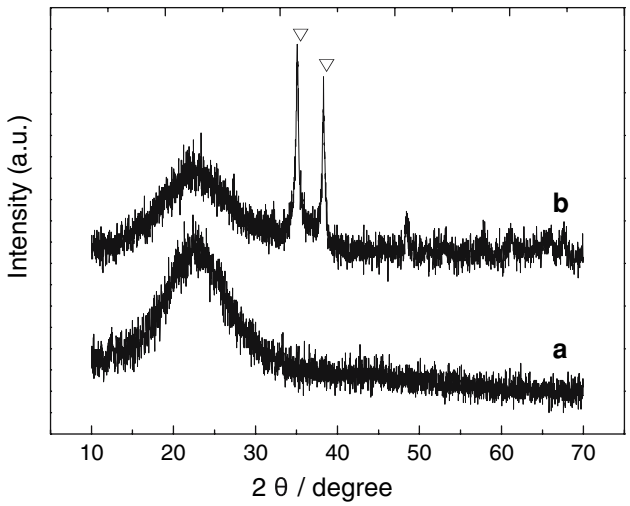


**Fig. 3** XRD patterns of the samples. (**a**) Cu-20 dried at 50 °C and (**b**) Cu-20 calcined at 500 °C

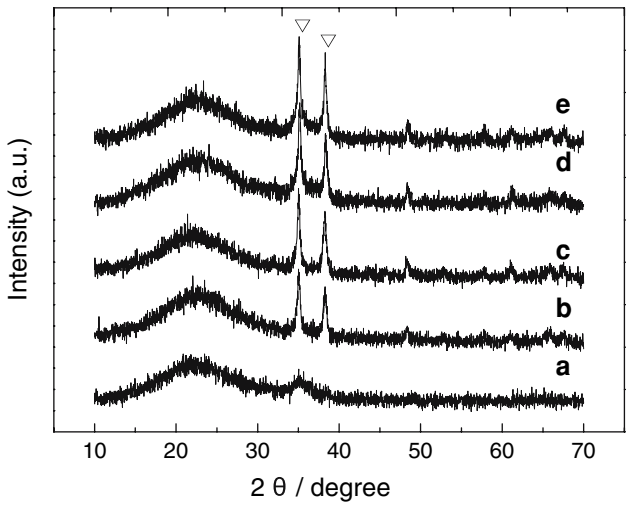


**Fig. 4** XRD patterns of $CuO/SiO_2$ samples calcined at 500 °C. (**a**) Cu-14R, (**b**) Cu-11, (**c**) Cu-14, (**d**) Cu-17, and (**e**) Cu-20. Peaks with open triangles are from CuO crystal

network with different structures. In the silica–alumina system, alumina is expected to be embedded in the silica network by forming Si–O–Al bonds [11]. However, it is not thought that copper can form the Si–O–Cu bond in the acidic conditions adapted in the present work. The copper ions in wet silica gel are probably extracted freely into the outer solution by a fast diffusion process. Therefore, most of the copper in the wet gel possibly exists in the solvent as an ion rather than in the gel network.

## Variation of the dispersion of CuO particles with CuO content

A water-soluble organic compound has ionic and/or polar functional groups, which can interact with inorganic

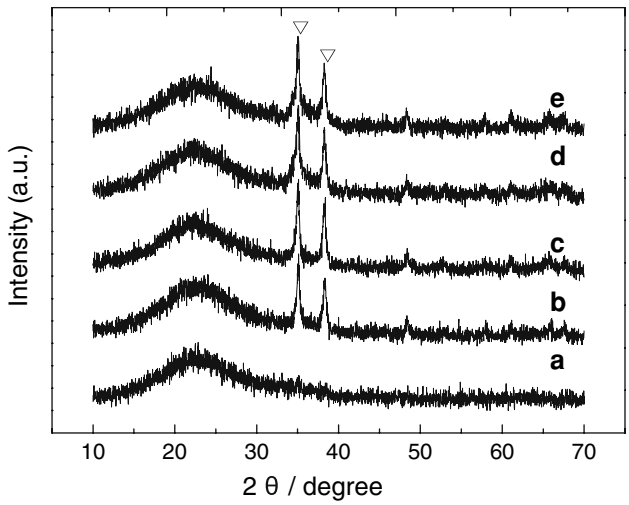


**Fig. 5** XRD patterns of $CuO/SiO_2$ samples reduced at 220 °C. (**a**) Cu-14R, (**b**) Cu-11, (**c**) Cu-14, (**d**) Cu-17, and (**e**) Cu-20. Peaks with open triangles are from CuO crystal

components. For example, ether oxygens in polyoxyethylene chain of PEO can form hydrogen bonding with silanol groups on silica [17]. They can also coordinate to various metal cations. Such interaction between organic compounds and metal cations decreases symmetricity of the coordination structure of the metal cation, leading to the decrease in crystallizability of its salt. Then, aggregation of metal cations in silica gel can be suppressed during drying because the driving force for the aggregation in drying is the crystallization of the metal salt. Just as reported in the nickel–silica system [12], the interaction of the Ni cation with the PEO inhibits the crystallization of Ni salt during drying. Thus, the Ni is selectively entrapped as small particles in the gel skeleton.

In contrast, the result of $CuO/SiO_2$ in our present work is quite different from that of $NiO/SiO_2$. As shown in Fig. 4 and Table 1, the diffraction peaks of CuO in the $CuO/SiO_2$ samples except for the Cu-14R are sharp, and the crystallite sizes of the CuO estimated from the peak width are not small as expected. This indicates no obvious interaction between the Cu cation and the PEO, most of the copper ions in wet silica gel are present in the outer solution. Then, they easily aggregate as copper salts in the drying process of wet gel and decompose into CuO particles in heating. This result is obviously shown in the samples with higher CuO content. As shown in Fig. 2, particle aggregation is observed in the macropores or on the gel skeleton in the Cu-17 and Cu-20 samples. But there is no much difference in the crystallite sizes of the CuO between Cu-17, Cu-20 and Cu-11, Cu-14 (Table 1). This is because the CuO particle size estimated from the XRD peak width is an average value. The Cu-11 and Cu-14 samples with low CuO content have homogeneous CuO particles, while the

Cu-17 and Cu-20 samples have large and small crystallite simultaneously. However, the peaks of CuO for the Cu-14R are much broader than those for the $CuO/SiO_2$ samples with the presence of PEO, and the crystallite size of the CuO estimated from the peak width in Fig. 4 is 7 nm, which is smaller than that of other $CuO/SiO_2$ samples. The result suggests that Cu cations in the Cu-14R sample can interact with silica gel network in the absence of PEO, which inhibits the move of Cu cations from the gel skeleton to the outer solution. Thus, the Cu is selectively entrapped as small particles in the gel skeleton. Although what interaction between Cu aqua complex and silica gel network has not been made clear, the existence of PEO can affect it.

## Conclusion

A $Cu/SiO_2$ catalyst is prepared by co-gelation using phase separation, which has distinct macropores and mesopores. The addition of copper into the silica–PEO system has a negligible effect on the morphology formation. The dispersion of CuO into such bimodal pores varies with CuO content. The crystallite sizes of the CuO estimated from the peak width in the $Cu/SiO_2$ with the presence of PEO are not small as expected. While the crystallite size of CuO in the $Cu/SiO_2$ with the absence of PEO is smaller than that of other $CuO/SiO_2$ samples. It is considered that the Cu is selectively entrapped as small particles in the gel skeleton due to the interaction between Cu aqua complex and silica gel network.

**Acknowledgement** The authors are grateful to the financial support from China Petrochemical Corp. (No. X504033).

## References

1. Sekizawa K, Yano S, Eguchi K, Arai H (1998) Appl Catal A 169:291
2. Fridman VZ, Davydov AA (2000) J Catal 195:20
3. Brands DS, Poels EK, Bliek A (1999) Appl Catal A 184:279
4. Ueno A, Suzuki H, Kotera Y (1983) J Chem Soc Faraday Trans 79:127
5. Miller J, Rankin S, Ko E (1994) J Catal 148:673
6. Nakanishi K, Soga N (1991) J Am Ceram Soc 74:2518
7. Nakanishi K, Komura H, Takahashi R, Soga N (1994) Bull Chem Soc Jpn 67:1327
8. Minakuchi H, Nakanishi K, Soga N, Ishizuka N, Tanaka N (1996) Anal Chem 68:3498
9. Nakanishi K, Motowaki S, Soga N (1992) Bull Inst Chem Res 70(2):144
10. Takahashi R, Nakanishi K, Soga N (1998) J Ceram Soc Jpn 106:772
11. Takahashi R, Sato S, Sodesawa T, Yabuki M (2001) J Catal 200:197
12. Nakamura N, Takahashi R, Sato S, Sodesawa T, Yoshida S (2000) Phys Chem Chem Phys 2:4983
13. Sato S, Takahashi R, Sodesawa T, Koubata M (2005) Appl Catal A 284:247
14. Ishizuka N, Minakuchi H, Nakanishi K, Soga N, Tanaka N (1998) J Chromatogr A 797:133
15. Nakanishi K, Komura H, Takahashi R, Soga N (1994) Bull Chem Soc Jpn 67:1327
16. Nakanishi K, Yamasaki Y, Kaji H, Soga N, Inoue T, Nemoto N (1994) J Sol-Gel Sci Technol 2:227
17. Takahashii R, Sato S, Sodesawa T, Suzuki M, Ogura K (2000) Bull Chem Soc Jpn 73:765